3D SEISMIC INTERPOLATION WITH A LOW REDUNDANCY, FAST CURVELET TRANSFORM

JINGJIE CAO[1] and JINGTAO ZHAO[2]

[1] *Shijiazhuang University of Economics, Shijiazhuang, Hebei 050031, P.R.China. cao18601861@163.com*
[2] *Research Institute of Petroleum Exploration & Development, PetroChina, Beijing 100083, P.R.China. diffzjt@163.com*

(Received October 25, 2014; revised version accepted December 12, 2014)

ABSTRACT

Cao, J. and Zhao, J., 2015. 3D seismic interpolation with a low redundancy, fast curvelet transform. *Journal of Seismic Exploration*, 24: 121-134.

Seismic data interpolation is one of the main challenges encountered during pre-processing. It can provide reliable data for processes that require regular and dense sampling, like migration and multiple elimination. At present, a transform method which is based on the sparseness of signals in a transformed domain, is a commonly used strategy to get promising results. Among different transforms, the curvelet transform has optimal sparse expression for wave-fronts, thus it can be seen as a good candidate for seismic interpolation. However, the high redundancy of the 3D curvelet transform makes it computationally expensive, especially for massive data processing. Woiselle et al. (2011) proposed a new implementation of the curvelet transform, which reduces the redundancy to 10 for a 3D transform. In this paper, this new implementation is introduced to improve the computational efficiency of curvelet-based interpolation. The merits of the new implementation are discussed and the low redundancy is proven through numerical tests. Numerical results on 3D interpolation based on the new transform show that the CPU time it costs is about 1/4 of the original curvelet transform. Thus, the Woiselle's curvelet transform is a good balance between redundancy, rapidity and performance.

KEY WORDS: curvelet transform, seismic interpolation, sparse optimization, one-norm.

INTRODUCTION

In seismic exploration, the sampled data often violates the Shannon sampling theorem due to acquisition costs, bad traces, topography and noise. The incomplete data may affect results of migration (Liu and Sacchi, 2004), denoising (Soubaras, 2004), multiple elimination (Naghizadeh, 2009) and AVO

0963-0651/15/$5.00

analysis (Sacchi and Liu, 2005). Seismic interpolation is a crucial method to provide reliable data from the incomplete data. Among various interpolation methods, signal processing-based methods play an important role to provide reliable wavefield information (Liu and Sacchi, 2004; Zwartjes and Gisolf, 2006; Herrmann and Hennenfent, 2008). Especially sparse transform methods constitute an important class, when data is assumed to be sparsely represented in a suitable transform domain. Besides the well-known Fourier transform (Liu and Sacchi, 2004; Zwartjes and Gisolf, 2006), Radon transform (Trad et al., 2002) and local Radon transform (Sacchi et al., 2004) are also commonly used. However, they all operate on a single scale and the decomposition into multi-resolution elements is not used. In the last decade, multi-scale methods have been gaining much interest, especially the curvelet transform. The curvelet transform was first proposed by Candès and Donoho (2000) as a new multi-scale, multi-directional and sparse representation of curve-like signals. The curvelets are localized not only in the spatial domain and the frequency domain, but also in angular orientation. A new important directional parameter provides an additional angular geometric property with a high degree of orientation which identifies the directional singularities (Candès and Donoho, 2004). As a multi-scale, multi-directional, anisotropic tight frame, it is strictly localized in Fourier domain. Furthermore, it provides an optimal representation of objects that have discontinuities along edges (Candès and Donoho, 2000; Starck et al., 2002; Candès and Donoho, 2004).

In seismic processing, the curvelet transform has been applied to interpolation (Herrmann et al., 2008a; Yang et al., 2013), denoising (Hennenfent and Herrmann, 2006), multiple attenuation (Herrmann et al., 2008b; Lin and Herrmann, 2013), deconvolution (Kumar and Herrmann, 2008) and migration (Chauris and Nguyen, 2008). Neelamani et al. (2008) introduced curvelet-based noise attenuation for 3D seismic data corrupted with random and linear noise. More seismic issues like ground roll attenuation (Yarham and Herrmann, 2008) or enhancing crystal reflection data with sparsity promotion (Kumar et al., 2011) were solved with curvelet-based methods proving their value for seismic processing.

Though the curvelet transform has plenty of merits for seismic processing, it is a highly redundant transform with redundancy up to a factor 24-32 for 3D signals. This is a crucial defect for large-scale data processing, which can increase computation time greatly. A low redundancy curvelet transform is proposed in Woiselle et al. (2011), which can reduce the redundancy to a factor 10 for 3D signals. This paper proposes to use this low redundancy curvelet transform as a replacement of the Candès curvelet transform for 3D data interpolation. The low redundancy of the new transform is proven by our analysis and utilized to accelerate computation. The structure of this paper is as follows, the basis theory and solving methods of seismic interpolation are introduced at first, and then the features of this transform are illustrated.

Numerical examples on interpolation using this new transform demonstrate the improvement of computation efficiency compared with the Candès curvelet transform. At last, we conclude that the new transform is a good candidate for massive data processing.

THEORY

The forward problem of interpolation can be expressed as:

$$Rx + \varepsilon = d \quad , \tag{1}$$

where R is the sampling matrix, x is the unknown seismic data, ε is the additive noise, and d is the sampled data. Since the sampled data is often incomplete and violates Shannon theorem, there are infinitely many solutions theoretically. However, according to regularization theory, if some *a priori* information is known at first, the ideal solution can be found correctly. Sparseness of solutions in some transform domain is commonly used since the unknown data can be expressed sparsely by some transforms. If $s = \Psi x$ is sparse, where Ψ is an operator that represents a sparse transform, then eq. (1) can be changed into

$$R\Psi^* s + \varepsilon = d \quad , \tag{2}$$

where Ψ^* is the conjugate transpose of Ψ. Based on the sparsity assumption of s, it can be obtained by solving the following optimization problem (Chen et al., 1998)

$$\min \| s \|_1 \text{s.t.} \ \| R\Psi^* s - d \|_2^2 \leq \sigma \quad , \tag{3}$$

where σ is an estimation of the noise energy. Here, the interpolation problem was transformed to an optimization problem that can be called a basis pursuit method (Chen et al., 1998). If s is solved, then x can be obtained by $x = \Psi^* s$. Besides the L_1-norm regularization, total variation regularization is another commonly used strategy for interpolation (Tang et al., 2012). For other regularization operators such as Cauchy norm, refer to Zwartjes and Gisolf (2007).

As for the solving methods of problem (3), it can be efficiently solved by the well-known iterative soft thresholding (IST) method (Daubechies et al., 2004) or iterative hard thresholding (IHT) method (Blumensath and Davies, 2008). Projection onto convex sets (POCS) method is an important method for seismic interpolation (Abma and Kabir, 2006). The above mentioned methods are all high efficient and robust when chosen proper parameters. For more methods of solving problem (3), refer to Cao et al. (2011).

An important aspect to improve solutions of problem (3) is choosing proper transforms, such as Fourier (Sacchi and Ulrych, 1996; Sacchi et al., 1998), Radon (Trad et al., 2002), seislet (Fomel and Liu, 2010) and curvelet transform (Herrmann et al., 2008a). The curvelet transform is an effective transform that allows sparse representations of complex data. This spectral technique is based on directional basis functions that represent objects having discontinuous along smooth curves. As a multi-scale, multi-directional and high dimension tight frame (Candès et al., 2006), the curvelet transform has excellent compression for wave-fronts (Herrmann et al., 2008a). However, its high redundancy, with a factor 24-32 redundancy for 3D data, costs much time in numerical computation. How to improve the efficiency of curvelet interpolation and keep its excellent compression ability is the start point of this paper. Woiselle et al. (2011) proposed a new implementation of the curvelet transform which can reduce the redundancy to a factor 10 for 3D data. In this paper, the low redundancy of Woiselle's curvelet transform is utilized to accelerate the speed of curvelet-based interpolation. The Woiselle curvelet transform is introduced in the next section.

A LOW REDUNDANCY CURVELET TRANSFORM IMPLEMENTATION

In order to clarify the merits of the Woiselle's curvelet transform, the implementation of a wrapping-based curvelet transform is introduced. Then, it is explained why the Woiselle's transform can reduce extra redundancy.

The 3D curvelet transform (Candès et al., 2006) consists of a low-pass approximation sub-band partition, and a family of curvelet sub-bands carrying the curvelet coefficients indexed by their scale, position and orientation (Woiselle et al., 2011). There are mainly two steps in the transform: multi-scale separation and angular separation. At first, the input 3D data with size $N = (N_x,N_y,N_z)$ is separated into dyadic corona based on the 3D Meyer wavelet transform in the Fourier domain using the compactly supported Fourier transform and get cubes of sizes N, N/2, ..., $N/2^J$, where J is the number of scales. Secondly, each corona is separated into anisotropic wedges of trapezoidal shape obeying the so-called parabolic scaling law. The curvelet coefficients are obtained by a 3D inverse Fourier transform applied to each wedge appropriately wrapped to fit 3D rectangular parallelepipeds.

In the original implementation, high redundancy comes mainly from the angular separation. Additionally, the way to apply the Meyer wavelet transform added extra redundancy. However, the new curvelet transform implementation can reduce the extra redundancy (Woiselle et al., 2011). There are many differences between the Woiselle's transform and the original one, but the main reason to reduce extra redundancy lies in the way the Meyer wavelet transform is applied to the data. More details of the Meyer wavelet transform implementation are discussed in the following.

The extra redundancy of the curvelet transform as implemented in Curvelab (Candès and Donoho, 2004) originates mainly from the way the radial window is implemented, especially the finest scale. Taking the 1D Meyer wavelet transform as an example, we call ψ_j the Meyer wavelet at scale $j \in \{0,\cdots,J-1\}$ and ϕ_{J-1} the scaling function at the coarsest scale, denoting $M_j = \hat{\psi}_j = 2^{-3j/2}\psi(2^{-j})$ and $M_J = \hat{\phi}_{J-1} = 2^{-3(J-1)/2}\hat{\phi}(2^{-2(J-1)})$ as their Fourier transforms. The Meyer wavelets $\hat{\psi}(\xi)$ are defined in the Fourier domain as follows:

$$\hat{\psi}(\xi) = \begin{cases} e^{-i2\pi\xi}\sin[(\pi/2)v(6|\xi|-1)] & , \quad 1/6 < |\xi| \le 1/3 \\ e^{-i2\pi\xi}\sin[(\pi/2)v(3|\xi|-1)] & , \quad 1/3 < |\xi| \le 2/3 \\ 0 & , \quad \text{elsewhere} \end{cases}, \tag{4}$$

where v is a smooth function that goes from 0 to 1 on [0,1] and which satisfies $v(x) + v(1-x) = 1$. The Meyer scaling functions are defined by

$$\hat{\phi}(\xi) = \begin{cases} 1 & , \quad |\xi| \le 1/6 \\ \cos[(\pi/2)v(6|\xi|-1)] & , \quad 1/6 < |\xi| \le 1/3 \\ 0 & , \quad |\xi| > 1/3 \end{cases}, \tag{5}$$

Fig. 1 displays in solid lines the graphs of the Fourier transform of the Meyer scaling and wavelet functions at three scales. The wavelet at the finest scale in the Fourier domain is supported on $[-2/3,-1/6]\cup[1/6,2/3]$, hence exceeding the Shannon band. The original curvelet transform implicitly assumes periodic boundary conditions. Moreover, it is known that computing the wavelet transform of a periodized signal is equivalent to decomposing the signal in a periodic wavelet basis. Thus, the exceeding end of the finest scale is replaced with its mirrored version around the vertical axis at $|\xi| = 1/2$, as shown in the dashed line in the top of Fig. 1. Consequently, the support of the data is 4/3 larger than the original one, hence boosting the redundancy by a factor $(4/3)^3$ in 3D. In the Woiselle's implementation, the supports of the scaling and wavelet functions were firstly shrunk by a factor of 4/3. Furthermore, in order to maintain the uniform of partition of unity, the finest scale wavelet is modified by suppressing its decreasing tail so that the wavelet becomes a constant over $[-1/2,-1/4]\cup[1/4,1/2]$. This added no extra redundancy for the 3D Meyer wavelet transform in the Fourier domain.

The redundancy is 24-32 for the original 3D curvelet transform, but the redundancy of Woiselle's implementation is only 10 for 3D (Woiselle et al., 2011). Besides the low redundancy while maintaining the directional selectivity property at the finest scale, this Woiselle's curvelet transform is isometric and with fast exact reconstruction, the proposed curvelet transform corresponds to a Parseval tight frame, i.e., $C^*C = I$, where C is the curvelet analysis operator and C^* its adjoint. Thus, C^* turns out to be also the inverse operator associated to a fast reconstruction algorithm.

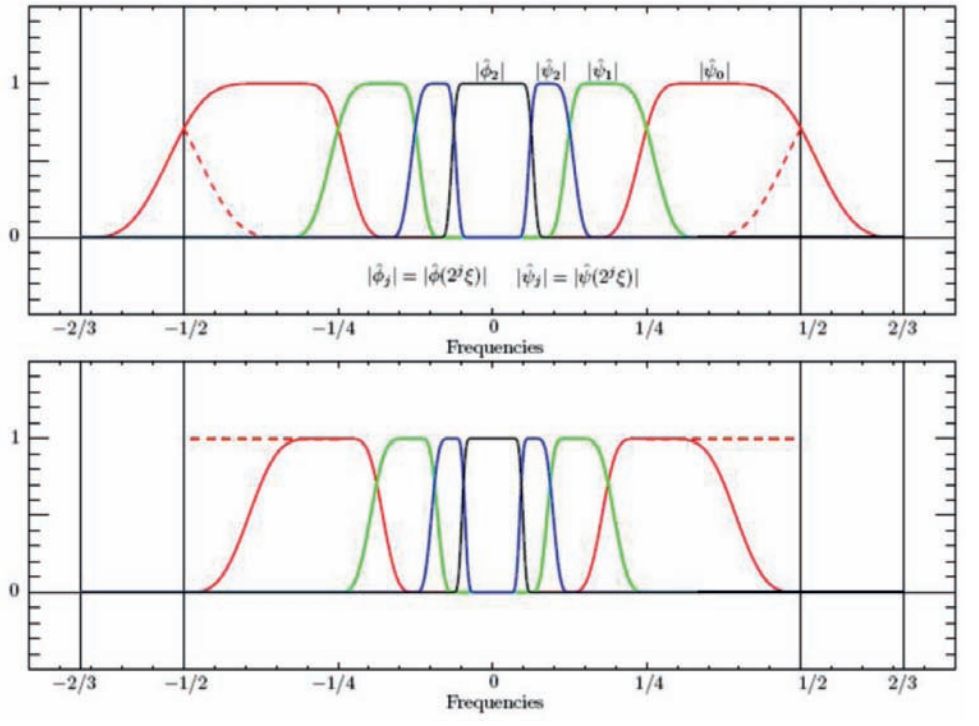

Fig. 1. Meyer scaling and wavelet functions in the 1D Fourier domain. Top: Meyer wavelet transform in the Candès curvelet transform. Bottom: Meyer transform in the Woiselle's implementation.

In order to test the redundancy of the Woiselle's curvelet transform numerically, a $64\times64\times64$ seismic cube is transformed by these two transforms with different scales and angles. For different scales and angles, the curvelets coefficient numbers and maximum absolute values are listed in Table 1. In the first row of the table, "3" means the scale number and "8" means the angle number at the second coarsest scale. In the second row of the table, "Candès" denotes the Candès curvelet transform, and "Woiselle" denotes the Woiselle's transform. In this table, the coefficient numbers of Woiselle's curvelet transform are about 2/5 of that of Candès curvelet transform for all scales and angles cases, and their max absolute values are bigger than the original one. This proved the low redundancy of the Woiselle's curvelet transform, which will greatly benefit the computational efficiency for massive data processing. Thus, this low redundancy will reduce CPU time during numerical computation of interpolation.

Table 1. Comparison of Candès curvelet transform and Woiselle's curvelet transform.

Scales and angles	(3,8)		(4,8)		(5,8)	
	Candès	Woiselle	Candès	Woiselle	Candès	Woiselle
Number of curvelet coefficients	6,932,397	2,958,281	7,199,027	3,008,529	8,380,925	3,015,701
Maximum absolute value	6.4089	17.3266	9.2697	36.7048	9.0650	32.3275

3D INTERPOLATION BASED ON THE WOISSELE'S CURVELET TRANSFORM

In this section, the efficiency of the Woiselle's curvelet transform to accelerate computation is evaluated on two examples. The well-known projection onto convex set (POCS) method is used to solve problem (3), and the iteration numbers are the same for these two transforms (Woiselle et al., 2011). For the first example, a synthetic seismic line is used to study the potential uplift for computational efficiency with the Woiselle's transform over the original one. The synthetic seismic line is simulated with a finite-difference code for a subsurface velocity model with two velocity layers. Using an acoustic finite-difference modeling algorithm, 64 shots and 64 receivers are simulated on a fixed receiver spread with receiver steps of 12 m. The time sample interval is 4 ms. Data generated by these simulations can be organized in a 3D data volume. Some papers show that interpolation of midpoint-offset shot gathers can get better results than midpoint-offset data, however, we'd like to interpolate source-receiver data because of its physical meaning. The full data is depicted in Fig. 2(a), and the incomplete acquisition with 50 percent receiver positions randomly sampled for each shot is shown in Fig. 2(b). The full data serves as the ground truth. The interpolation result using the Woiselle's transform is plotted in Fig. 2(c) with Fig. 2(d) showing the difference between the original data and interpolated data. In order to test the interpolation performance for further reduced sampling, an incomplete data with a sampling ratio of 20%, meaning with 80 percent receivers randomly removed for each shot, is depicted in Fig. 3(b), and the interpolation result based on the Woiselle's transform is shown in Fig. 3(c), the difference between the original data and the interpolated data is shown in Fig. 3(d). More results of these two transforms based interpolation are listed in Table 2, where SNR is defined as $\mathrm{SNR} = 10\log_{10} \times [\| x_{orig} \|_2^2 / \| x_{orig} - x_{rest} \|_2^2]$, x_{orig} is the complete data and x_{rest} is the interpolated data. From Table 2, it can be observed that the CPU time using the Woiselle's transform is about 1/4 of the original one. Furthermore, the SNR of them are comparable.

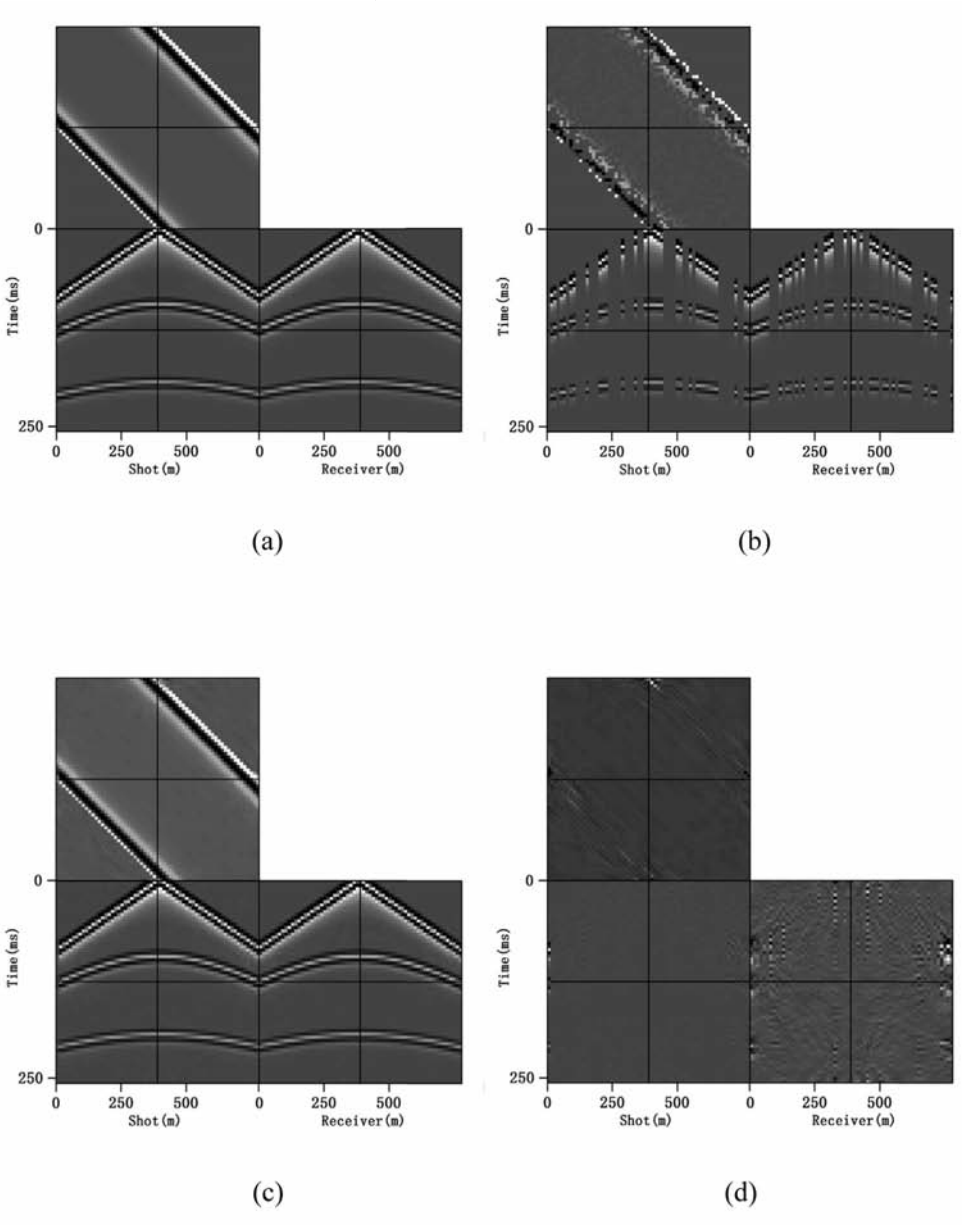

Fig. 2. (a) Complete data cube consisting of 64 x 64 x 64 samples along the source, receiver and time coordinates. (b) Simulated acquired data with 50 percent randomly missing traces. (c) Interpolation of 50% sampled data using the new transform. (d) Difference between the interpolated data and the original data.

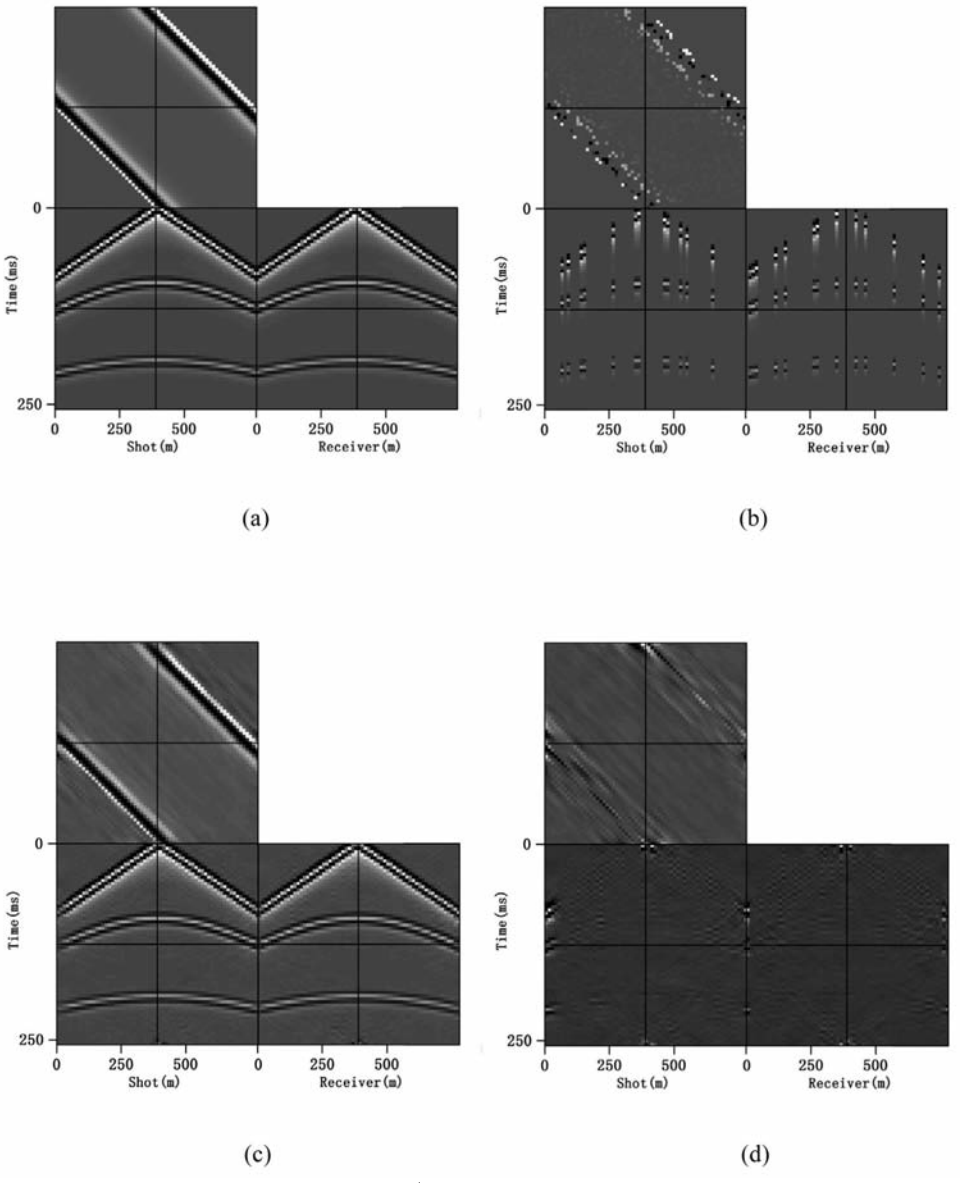

Fig. 3. (a) Same data cube as in Fig. 2(a). (b) Simulated acquired data with 80% traces randomly missing. (c) Interpolation of 20% sampled data using the new transform. (d) Difference between the interpolated data and the original data.

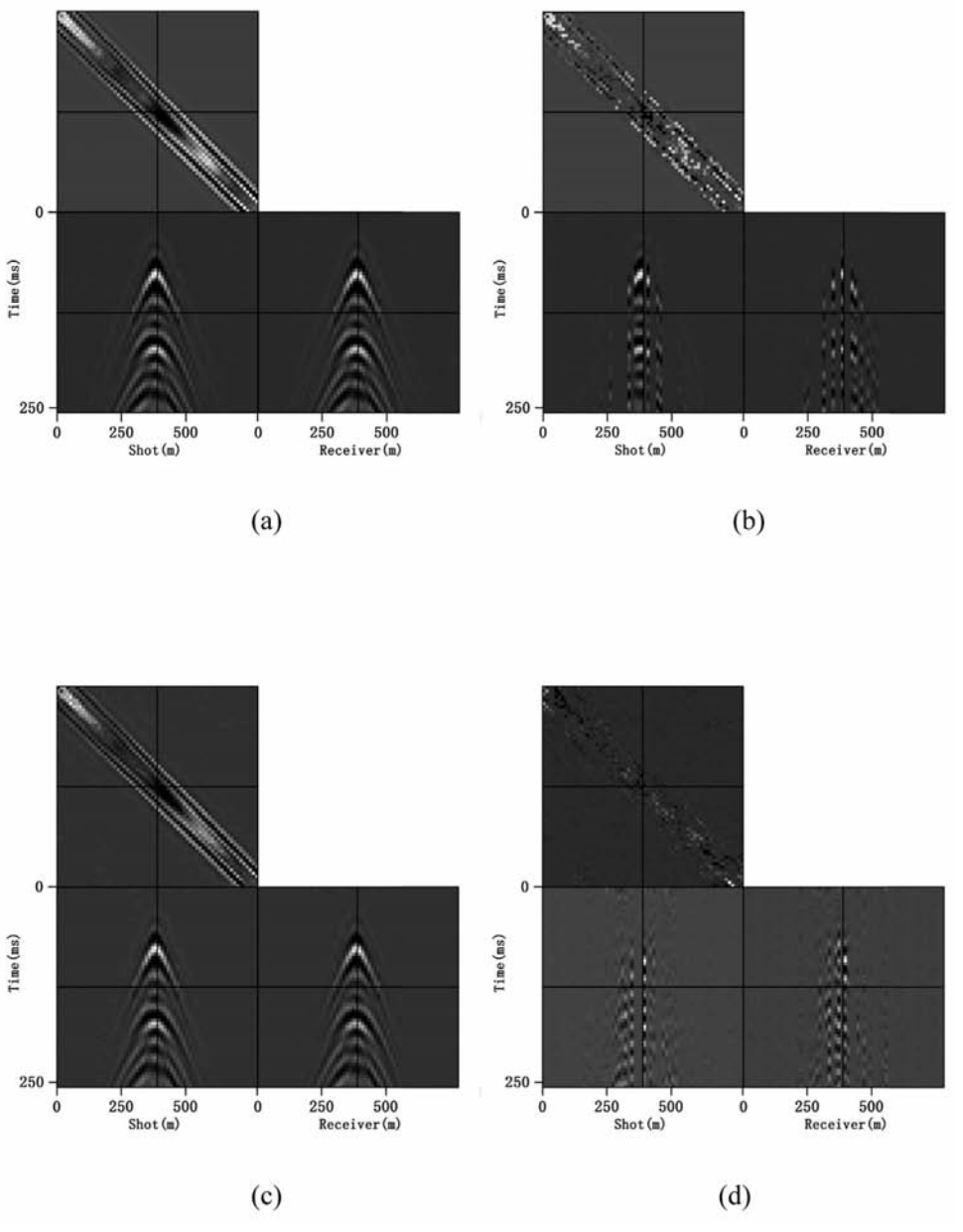

Fig. 4. (a) Complete data cube consisting of 64 x 64 x 64 samples along the source, receiver and time coordinates from finite difference simulation. (b) Simulated acquired data with 50% randomly missing traces. (c) Interpolation of 50% sampled data using the new transform. (d) Difference between the interpolated data and the original data.

Table 2. Interpolation of these two transforms for Data1 with different sampling ratio.

Sampling ratio	50%		20%		10%		5%	
	Candès	Woiselle	Candès	Woiselle	Candès	Woiselle	Candès	Woiselle
CPU time (s)	1066	176	756	190	759	176	1082	271
SNR (dB)	20.3365	30.2013	13.5222	17.1638	8.7660	10.3631	4.1165	7.6232

Table 3. Comparison of these two curvelet transforms for Data2.

Transform	Candès	Woiselle
CPU time (s)	789	178
SNR (dB)	15.4602	14.4105

Another interpolation example is given to test the efficiency of the Woiselle's transform further. Data2 with size $64\times64\times64$ is generated using a finite-difference method. The time and space interval are the same as Data1. Fig. 4(a) is the original Data2, Fig. 4(b) depicts the data with 50 percent randomly missing traces, Fig. 4(c) is the interpolated data using the Woiselle's transform and Fig. 4(d) is the difference between the original data and the interpolated data. The SNR and CPU time for interpolation using these two transforms are listed in Table 3. The time consumption of the Woiselle's transform is also about 1/4 of the original one, however, the SNR of interpolation is smaller than the original one, which may caused by the scale separation of the Woiselle's implementation. This example again proved the efficiency promotion of the Woiselle's transform, which means that it is a good comprise between redundancy, rapidity and performance.

In the following, field data is used to test the interpolation quality of the new curvelet transform, the size of the field data is $1024\times128\times128$, which means the time sampling number is 1024, the in-line and cross-line numbers are 128. A small time window is chosen, and the random sampling number is 1/4 of the total traces. Fig. 5(a) is an in-line slice of the field data, Fig. 5(b) is the sampled version of this slice, and Fig. 5(c) is the new curvelet-based interpolation. Fig. 6(a) is a cross-line slice of the field data, Fig. 6(b) is the sampled version of this slice, and Fig. 6(c) is the new curvelet-based interpolation. Fig. 7(a) is a time slice of the field data, Fig. 7(b) is the sampled version of Fig. 7(a), and Fig. 7(c) is the new curvelet-based interpolation. The SNR of the restoration is 26.8581, so the new curvelet transform can also be suitable for filed data.

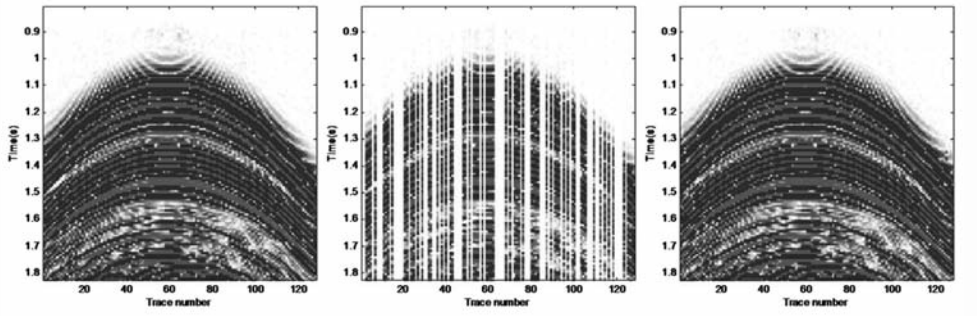

Fig. 5. (a) A in-line slice of the field 3D data, (b) its sampling version, (c) the new curvelet-based interpolation.

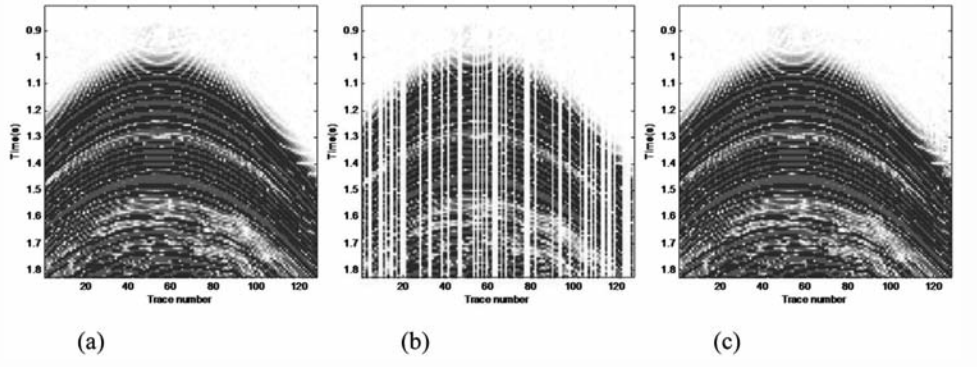

Fig. 6. (a) A cross-line slice of the field 3D data, (b) its sampling version, (c) the new curvelet-based interpolation.

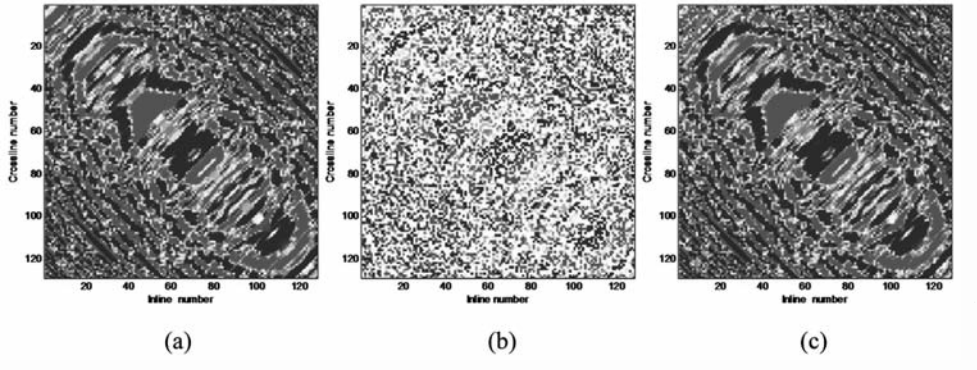

Fig. 7. (a) A time slice of the field 3D data, (b) its sampling version, (c) the new curvelet-based interpolation.

CONCLUSIONS AND DISCUSSION

In this paper, Woiselle's curvelet transform, which reduces the redundancy to a factor 10 for 3D data, is introduced to improve the efficiency of curvelet transform-based interpolation. The main reason why the Woiselle's transform can reduce redundancy lies in the way the Meyer wavelet transform is applied to the data. This merit renders it very suitable for massive data processing. Numerical examples proved that the Woiselle's transform costs 1/4 CPU time of the original one for interpolation when getting comparable results, which means that it is a good balance between redundancy, rapidity and performance. In all, it can be seen as a good candidate for massive seismic data processing.

Since the curvelet transform is based on the Fourier transform, using it solely can not treat regular sampled data interpolation. Because of the memory restriction of the used computer, small sizes of data are considered, but this is no hamper to prove the computation efficiency of the new transform. Since the truncation in the implementation, the interpolation efficiency is improved; however, the quality of the interpolation may a little worse than the original Candès transform in some cases. A transform which can get a good trade-off between redundancy, optimality of transform, level of sparsity, and recover condition is no doubt benefits a lot for interpolation. However, this problem is still open, and more transforms should be compared to get further conclusions.

ACKNOWLEDGMENTS

We acknowledge WesternGeco for providing the Mississippi Canyon data. We thank Prof. Eric Verschuur for his constructive comments and suggestions. We would also like to thank the authors of Curvelab for making their codes available. This work is supported by National Natural Science Foundation of China under grant numbers 41204075, grant of China Scholarship Council, Natural Science Foundation of Hebei Province under grant number D2014403007 and Young Talents of Universities in Hebei Province under grant number BJ2014049.

REFERENCES

Abma, R. and Kabir, N., 2006. 3D interpolation of irregular data with a POCS algorithm. Geophysics, 71: E91-E97.

Beckouche, S. and Ma, J., 2014. Simultaneous dictionary leanring and denoising for seismic data. Geophysics, 79: A27-A31.

Blumensath, T. and Davies, M., 2008. Iterative thresholding for sparse approximations. J. Fourier Analys. Appl., 14: 629-654.

Candès, E., Demanet, L., Donoho, D. and Ying, L., 2006. Fast discrete curvelet transforms. Multiscale. Model. Sim., 5: 861-899.

Candès, E. and Donoho, D., 2000. Curvelets - A surprisingly effective nonadaptive representation for objects with edges. Vanderbilt Univ. Press: 105-120.

Candès, E. and Donoho, D., 2004. New tight frames of curvelets and optimal representation of objects with piecewise C2 singularities. Communic. Pure Appl. Mathemat., 57: 219-266.

Cao, J., Wang, Y., Zhao, J. and Yang, C., 2011. A review on restoration of seismic wavefields based on regularization and compressive sensing. Inverse Prob. Sci. Engin., 19: 679-704.

Chauris, H. and Nguyen, T., 2008. Seismic demigration/migration in the curvelet domain. Geophysics, 73: S35-S46.

Chen, S., Donoho, D. and Saunders, M., 1998. Atomic decomposition by basis pursuit. SIAM J. Sci. Comput., 20: 33-61.

Daubechies, I., Defrise, M. and Mol, C.D., 2004. An iterative thresholding algorithm for linear inverse problems with a sparsity constraint. Communic. Pure Appl. Mathemat., 57: 1413-1457.

Fomel, S. and Liu, Y., 2010. Seislet transform and seislet frame. Geophysics, 75(3): V25-V38.

Hennenfent, G. and Herrmann, F., 2006. Seismic denoising with non-uniformly sampled curvelets. Comput. Sci. Engin., 8: 16-25.

Herrmann, F. and Hennenfent, G., 2008. Non-parametric seismic data recovery with curvelet frames. Geophys. J. Internat., 173: 233-248.

Herrmann, F., Moghaddam, P. and Stolk, C., 2008a. Sparsity- and continuity-promoting seismic image recovery with curvelet frames. Appl. Comput. Harmon. Anal., 24: 50-173.

Herrmann, F., Wang, D., Hennenfent, G. and Moghaddam, P., 2008b. Curvelet-based seismic data processing: a multiscale and nonlinear approach. Geophysics, 73(1): A1-A5.

Kumar, V. and Herrmann, F., 2008. Deconvolution with curvelet-domain sparsity. Expanded Abstr., 78th Ann. Internat. SEG Mtg., Las Vegas: 1996-2000.

Kumar, V., Oueity, J., Clowes, R.M. and Herrmann, F., 2011. Enhancing crustal reflection data through curvelet denoising. Tectonophysics, 508: 106-116.

Lin, T. and Herrmann, F., 2013. Robust estimation of primaries by sparse inversion via one-norm minimization. Geophysics, 78(3): R133-R150.

Liu, B. and Sacchi, M., 2004. Minimum weighted norm interpolation of seismic records. Geophysics, 69: 1560-1568.

Naghizadeh, M., 2009. Parametric reconstruction of multidimensional seismic records. Ph.D. thesis University of Alberta, Edmonton.

Neelamani, R., Baumstein, A., Gillard, D., Hadidi, M. and Soroka, W., 2008. Coherent and random noise attenuation using the curvelet transform. The Leading Edge, 27: 240-248.

Sacchi, M. and Liu. B., 2005. Minimum weighted norm wavefield reconstruction for AVA imaging. Geophys. Prosp., 53: 787-801.

Sacchi, M. and Ulrych, T., 1996. Estimation of the discrete Fourier transform, a linear inversion approach. Geophysics, 61: 1128-1136.

Sacchi. M. and Verschuur, D. and Zwartjes, P., 2004. Data reconstruction by generalized deconvolution. Expanded Abstr., 74th Ann. Internat. SEG Mtg., Denver: 1989-1992.

Sacchi, M., Ulrych, T. and Walker, C., 1998. Interpolation and extrapolation using a high resolution discrete Fourier transform. IEEE T. Signal Process., 46: 31-38.

Soubaras, R., 2004. Spatial interpolation of aliased seismic data. Expanded Abstr., 74th Ann. Internat. SEG Mtg., Denver: 1167-70.

Starck, J., Candès, E. and Donoho, D., 2002. The curvelet transform for image denoising. IEEE Trans. Image Process., 11: 670-684.

Trad, D., Ulrych, T. and Sacchi, M., 2002. Accurate interpolation with high-resolution time-variant Radon transforms. Geophysics, 67: 644-656.

Tang, G., Ma, J. and Yang, H., 2012. Seismic data denoising based on learning-type overcomplete dictionaries. Appl. Geophys., 9: 27-32.

Woiselle, A., Starck, J. and Fadili, J., 2011. 3D Data denoising and inpainting with the low-redundancy fast curvelet transform. J. Math. Imaging. Vis., 39: 121-139.

Yang, P., Gao, J. and Chen, W., 2012. Curvelet-based POCS interpolation of nonuniformly sampled seismic records. J. Appl. Geophys., 79: 90-99.

Yarham, C. and Herrmann, F., 2008. Bayesian ground-roll separation by curvelet-domain sparsity promotion. Expanded Abstr., 78th Ann. Internat. SEG Mtg., Las Vegas: 3662-3666.

Zwartjes, P. and Gisolf, A., 2006. Fourier reconstruction of marine-streamer data in four spatial coordinates. Geophysics, 71(6): V171-V186.

Zwartjes, P. and Gisolf, A., 2007. Fourier reconstruction with sparse inversion. Geophys. Prosp., 55: 199-221.